A novel calcium-sensitive switch revealed by the structure of human S100B in the calcium-bound form

ARTICLE *in* STRUCTURE · MARCH 1998

Impact Factor: 5.62 · DOI: 10.1016/S0969-2126(98)00022-7 · Source: PubMed

2 AUTHORS:

Steven P Smith
Queen's University
52 PUBLICATIONS **872** CITATIONS
SEE PROFILE

Gary S Shaw
The University of Western Ontario
107 PUBLICATIONS **2,684** CITATIONS
SEE PROFILE

A novel calcium-sensitive switch revealed by the structure of human S100B in the calcium-bound form

Steven P Smith and Gary S Shaw*

Background: S100B is a homodimeric member of the EF-hand calcium-binding protein superfamily. The protein has been implicated in cellular processes such as cell differentiation and growth, plays a role in cytoskeletal structure and function, and may have a role in neuropathological diseases, such as Alzheimers. The effects of S100B are mediated via its interaction with target proteins. While several studies have suggested that this interaction is propagated through a calcium-induced conformational change, leading to the exposure of a hydrophobic region of S100B, the molecular details behind this structural alteration remain unclear.

Results: The solution structure of calcium-saturated human S100B (Ca^{2+}–S100B) has been determined by heteronuclear NMR spectroscopy. Ca^{2+}–S100B forms a well defined globular structure comprising four EF-hand calcium-binding sites and an extensive hydrophobic dimer interface. A comparison of Ca^{2+}–S100B with apo S100B and Ca^{2+}–calbindin D_{9k} indicates that while calcium-binding to S100B results in little change in the site I EF-hand, it induces a backbone reorientation of the N terminus of the site II EF-hand. This reorientation leads to a dramatic change in the position of helix III relative to the other helices.

Conclusions: The calcium-induced reorientation of calcium-binding site II results in the increased exposure of several hydrophobic residues in helix IV and the linker region. While following the general mechanism of calcium modulatory proteins, whereby a hydrophobic target site is exposed, the 'calcium switch' observed in S100B appears to be unique from that of other EF-hand proteins and may provide insights into target specificity among calcium modulatory proteins.

Address: Department of Biochemistry and McLaughlin Macromolecular Structure Facility, The University of Western Ontario, London, Ontario, N6A 5C1, Canada.

*Corresponding author.
E-mail: shaw@merlin.biochem.uwo.ca

Key words: calcium-binding protein, conformational change, human S100B, NMR, solution structure

Received: **27 October 1997**
Revisions requested: **24 November 1997**
Revisions received: **15 December 1997**
Accepted: **18 December 1997**

Structure 15 February 1998, **6**:211–222
http://biomednet.com/elecref/0969212600600211

Introduction

Calcium acts as a second messenger in a variety of cellular processes including cell division and growth, muscle contraction and enzymatic activation. One mechanism by which the calcium signal is propagated is through binding to calcium modulatory proteins. The EF-hand protein family [1] is one such class of calcium-binding proteins displaying several modes of calcium signalling via interaction with target proteins [2]. While a common theme is apparent to the different modes of signalling (i.e. the exposure of a hydrophobic surface), the mechanism by which this surface is provided is not synonymous. For example, calcium binding to the muscle contractile protein troponin C modifies its interaction with troponin I through a reorientation of two helices in its regulatory N-terminal domain [3,4]. This alteration in conformation is triggered by a simple transition in the ϕ and ψ backbone angles of Glu41, the z coordinating residue in one of the calcium-binding loops. Conversely, the ubiquitous protein calmodulin undergoes a massive reorientation of helices in both its N- and C-terminal domains upon calcium binding [5–8]. These conformational changes result in the exposure of several methionine residues where myosin light chain kinase (MLCK), caldesmon, and glycoprotein 41 can interact [9–11]. A third calcium modulatory protein, the visual sensor recoverin, undergoes a reorientation of helices at the interface of its two domains extruding its N-terminal myristoyl group from the hydrophobic cavity of the protein and allowing it to associate with the membrane bilayer [12–15].

One important class of EF-hand calcium-binding proteins where the mode of signalling has not been elucidated is the S100 protein family. This family comprises small (10–12 kDa), acidic, dimeric proteins which are expressed in a cell-specific manner and have been implicated in such roles as cellular growth and differentiation, cell-cycle regulation, and cytoskeletal function and structure [16–19]. Each S100B monomer (β) comprises a globular domain containing two EF-hand calcium-binding sites. Sequence comparison of the S100 proteins reveals the presence of a basic N-terminal pseudo (ψ) EF-hand

calcium-binding motif, comprising 14 residues (site I), and the more common acidic 12-residue canonical helix-loop-helix calcium-binding site in the C terminus (site II). The region joining the two calcium-binding sites (linker) and the extreme N- and C-terminal regions of the S100 family members appear more sequentially divergent. Several members of the S100 protein family display an increase in hydrophobic character upon calcium binding, the connecting trademark for calcium modulatory proteins, although to date there has been no definitive evidence for a mechanism showing how this occurs. One exception to this rule is the S100 family member calbindin D_{9k}, which is shorter in length than all other S100 proteins and exists as a monomer in solution. Unlike other calcium modulatory proteins, the three-dimensional structures of apo [20] and calcium-bound [21] calbindin D_{9k} reveal only a minor conformational change upon calcium-binding. This observation, in addition to the sequence divergence, have led to proposals that the linker and C terminus of the dimeric S100 proteins are responsible for their calcium-sensitive target recognition [22]. A further differentiating feature of several S100 proteins is a functional reliance on zinc through an increase in calcium affinity [23,24]. For example, protein kinase activation by S100A1 of the myosin-associated protein twitchin is increased more than 30-fold in the presence of zinc [25]. The zinc-binding sites in the S100 proteins have not been defined, however.

One important member of the S100 protein family is S100B, found primarily in the cytoplasm of glial cells [26]. Elevated expression of S100B has been observed in Alzheimer-afflicted patients, particularly in the regions of the brain where neuritic plaques have been localized, leading to the suggestion that S100B may have a role in this neuropathological disease [27–29]. In the absence of further evidence, it has been proposed that S100B undergoes a calcium-sensitive conformational change allowing it to interact with a variety of other target proteins. Thus, calcium-binding to S100B regulates interactions with tubulin [30,31] and glial fibrillary acidic protein (GFAP) [32], which are important for cellular architecture, and inhibits the phosphorylation of neuromodulin [33,34], myristoylated alanine-rich C kinase substrate (MARCKS) [35] and tau proteins [36,37] through interaction with the substrate. Recently, the three-dimensional structures of the calcium-free (apo) forms of rat [38] and bovine S100B [39] and rabbit S100A6 (calcyclin) [40] have been determined by nuclear magnetic resonance (NMR) spectroscopy. These structures demonstrate that the two monomeric S100 subunits, each comprising two helix-loop-helix EF-hand calcium-binding motifs, form a compact, globular, non-covalent homodimer in solution.

In this work we have determined the three-dimensional structure of human calcium-bound S100B (Ca^{2+}–S100B). This is the first structural report of a human S100 protein. A comparison of this structure with the NMR structures of rat apo S100B [38] and apo and calcium-bound calbindin D_{9k} [20,21] has allowed for a detailed analysis of the calcium-induced conformational changes of S100B. Specifically, calcium-binding appears to cause minimal changes in the site I pseudo EF-hand calcium-binding motif. However, the reorientation of N-terminal residues in the site II calcium-binding loop results in a significant change in the position of one helix, helix III, relative to the other helices. This helix rearrangement gives rise to the increased exposure of hydrophobic residues found at the C terminus of helix IV and in the linker. Based on their location, these exposed residues offer an attractive putative target-recognition site. These results provide structural evidence for previous biophysical observations and provide insight into the mode of calcium-sensitive target protein recognition for this family of proteins.

Results and discussion

It has previously been shown that calcium-binding to S100B has a strong salt dependence. In particular, S100B self-association occurs in the presence of calcium at higher ionic strengths, which gives rise to extensive broadening of NMR line widths [41,42]. This observation is consistent with the increased exposure of hydrophobic residues in Ca^{2+}–S100B as suggested by fluorescence and absorption studies [43–45]. Addition of the hydrophobic solvent trifluoroethanol (TFE) alleviated this effect in a manner similar to that observed in studies performed on calcium-saturated troponin C [46], or in studies using the detergent CHAPS (3-[3-cholamidopropyl)-dimethylammonio]-1-propane sulfonate) with calcineurin [47]. In the case of troponin C, comparison of the solution structure and crystal structure indicated that TFE had no effect on the folding of the protein [48]. Therefore, NMR samples used in this study were of low ionic strength and contained 10% TFE to minimize line broadening due to calcium-induced aggregation.

Description of the structure

The three-dimensional structure of human Ca^{2+}–S100B has been determined using 2574 experimental restraints obtained by multidimensional NMR spectroscopy (Table 1). Stereo views of the ensemble of the 20 low-energy structures of Ca^{2+}–S100B are shown in Figures 1a and 1b. The structures comprise two S100β monomers, each consisting of four α helices and a single β sheet. The symmetric relationship between the monomers is evident from a twofold rotational axis passing through the dimer interface approximately perpendicular to helices I and I′ and parallel to helices IV and IV′. NMR spectra were consistent with this symmetric nature as only one set of resonances was observed for most peaks [49]. The exception to this was the resonances for residues S1–A6, where some peak-doubling arose due to N-terminal chemical heterogeneity [50].

Table 1

Structural statistics for the 20 structures of Ca^{2+}–S100B.

Rmsd from experimental distance restraints (Å)*	
all (2344)	0.014 ± 0.001
intraresidue (1140)	0.011 ± 0.002
interresidue sequential (|i – j| = 1) (528)	0.014 ± 0.002
interresidue short range (1 < |i – j| < 5) (418)	0.018 ± 0.002
interresidue long range (|i – j| > 5) (150)	0.017 ± 0.004
intermolecular (40)	0.007 ± 0.002
hydrogen bond (68)	0.012 ± 0.002
Rmsd from experimental dihedral restraints (°) (230)	0.17 ± 0.045
Rmsd from idealized covalent geometry	
bonds (Å)	0.0014 ± 0.0001
angles (°)	0.2076 ± 0.0145
impropers (°)	0.1963 ± 0.0140
Energies (kcal mol $^{-1}$)	
E_{NOE}†	23.0 ± 4.7
E_{cdih}†	0.420 ± 0.22
E_{repel}‡	24.5 ± 4.0
E_{L-J}§	–504.2 ± 65.1
Rmsd of 20 structures relative to energy minimized average dimer structure (Å)	
backbone residues in secondary structure (backbone atoms/ all heavy atoms)#	0.68 ± 0.11/1.36 ± 0.11
all backbone residues (backbone atoms/ all heavy atoms)¶	1.35 ± 0.17/2.18 ± 0.22
Pairwise rmsd between monomer A and monomer B (Å)¥	
backbone residues in secondary structure	0.338
all backbone residues	0.678

*Root mean square deviation (rmsd) values are the average ± standard deviation for the best 20 low-energy structures; the number of each type of restraint used in the structure calculation is given in parentheses. †E_{NOE} and E_{cdih} were calculated using force constants of 50 kcal mol^{-1} Å^{-2} and 200 kcal mol^{-1} rad^{-2}, respectively. ‡E_{repel} was calculated using a final value of 4.0 kcal mol^{-1} Å^{-4} with the van der Waals hard sphere radii set to 0.75 times those in the parameter set PARALLHDG supplied by X-PLOR [85]. §E_{L-J} is the Lennard–Jones van der Waals energy calculated with the CHARMM empirical energy function and is not included in the target function for simulated-annealing calculations. #The calculation included the backbone Cα, N, and C′ atoms in the four helices and the two β strands for each of the monomers (Glu2–Tyr17, Lys26–Lys28, Ser30–Glu39, Val52–Glu58, Glu67–Asp69, Phe70–Phe87). ¶The calculation involved all residues including those found in the two calcium-binding loops and the linker region where a low number of restraints were identified. ¥Mean monomer structures were calculated from the ensemble of 20 dimer structures.

Each S100β monomer is formed by two helix-loop-helix EF-hand calcium-binding motifs joined by a flexible linker region (Figure 1). The N-terminal pseudo (ψ) EF-hand consists of helix I (Glu2–Tyr17), calcium-binding loop I (Ser18–Lys29) and helix II (Ser30–Glu39); the C-terminal canonical EF-hand comprises helix III (Val52–Glu58), calcium-binding loop II (Asp61–Asp69) and helix IV (Phe70–Phe88). Each calcium-binding loop contains a short antiparallel β strand (Lys26–Lys28; Glu67–Asp69). As is evident in Figure 1, the eight individual helices are very well defined individually (root mean square deviation [rmsd] ~0.32 Å) and the relative orientation of all secondary structure elements in the dimer is also well defined (rmsd ~0.68 Å). Although non-crystallographic symmetry (NCS) and distance symmetry were not employed at any point in the dimer structure calculations, the pairwise rmsd between the two mean monomer structures for all backbone atoms is still excellent (rmsd ~0.68 Å) indicating that symmetry is maintained to a very high degree among the monomers. The four calcium-binding loops are less well defined than the individual helices (rmsd of the ensemble relative to the average structure for loop I ~0.76 Å, and for loop II ~0.67 Å) while the linker regions between the two EF-hand calcium-binding motifs (Ser41–Glu51) are poorly defined. These findings are in agreement with the observed rapid amide exchange, relative to the helices, of residues Gly19–His25 (N terminus of loop I), Asp61–Gly66 (N terminus of loop II) and Ser41–Glu51 (linker) of Ca^{2+}–S100B. Similar observations have been noted for the analogous regions in loops I and II in calcium-saturated calbindin D_{9k} (Ca^{2+}–calbindin D_{9k}) which are generally poorly defined with respect to the helices and exhibit faster amide exchange [51]. In addition, the less well defined calcium-binding loops could result from the lack of long-range nuclear Overhauser effects (NOEs) involving these regions as well as the use of only a small number of dihedral restraints. The structural quality of Ca^{2+}–S100B is summarized in Table 1. In general this data shows small deviations from experimental restraints and uniformly low NOE and dihedral energies, indicating that the 20 solution structures are in good agreement with experimental data. Ramachandran analysis using PROCHECK [52] indicated that 93% of all residues, including the poorly defined regions, fell within the allowed regions of ϕ,ψ space.

The monomeric subunit of Ca^{2+}–S100B (S100β) is relatively compact and globular with the overall secondary structure content being very similar to that determined for apo S100B [38,39], apo S100A6 [40], and apo [20] and Ca^{2+}–calbindin D_{9k} [21]. The close proximity of the two EF-hands in each monomer is maintained by an antiparallel β sheet formed by two three-residue stretches in each of the calcium-binding loops (Lys26–Lys28; Glu67–Asp69). NOE evidence also showed that extensive hydrophobic interactions occur between the four helices. These interactions include contacts between residues from helices I and II (Phe14–Leu35), loop I and helix II (Leu27–Leu32), helices II and III (Leu32–Leu60), and from residues in helices I and IV (Phe14–Phe70 and Phe73) and III and IV (Leu60 to Val80). The arrangement of the four helices in S100β (Table 2) exhibits some

Figure 1

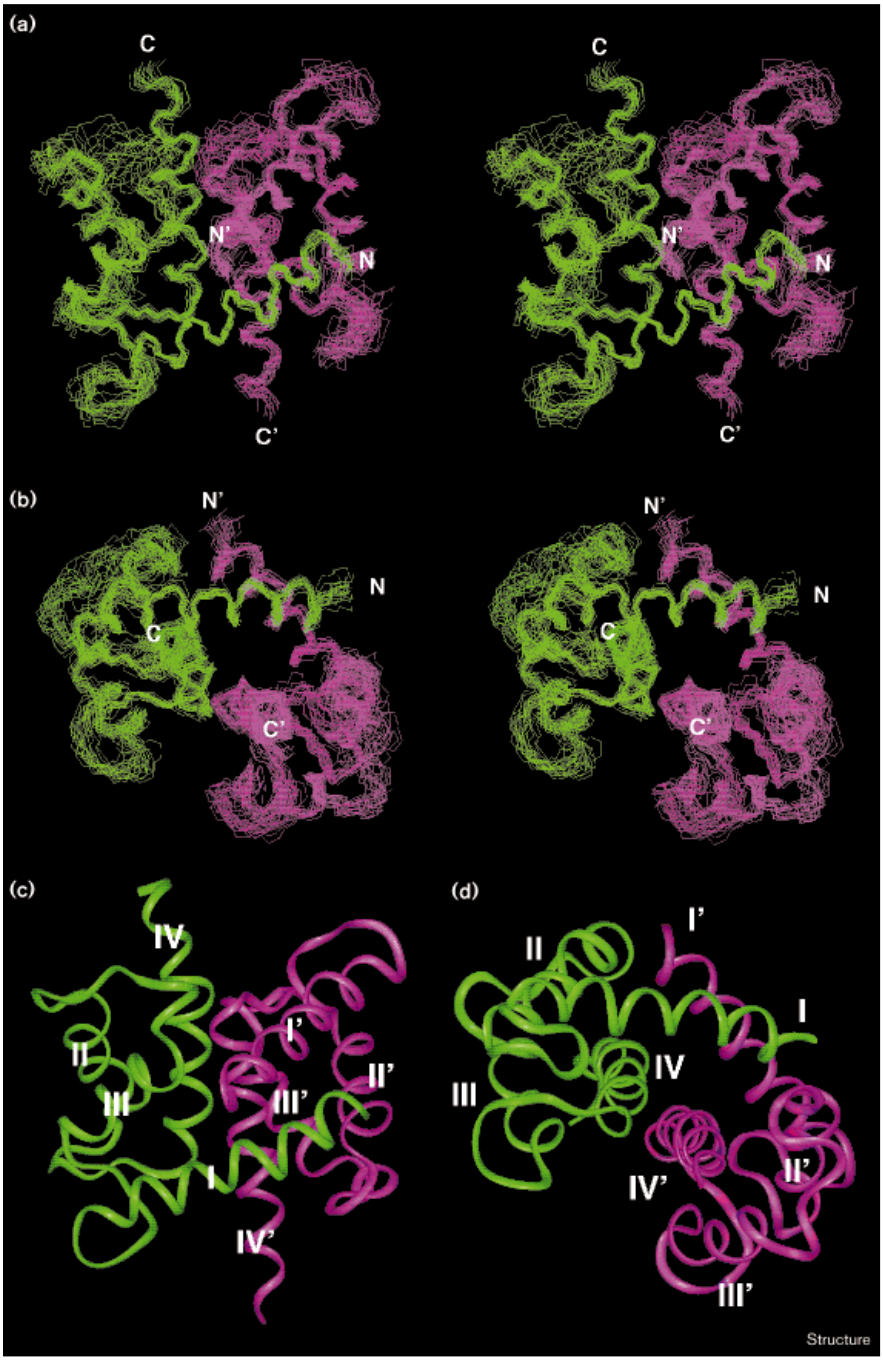

Structures of calcium-bound human S100B (Ca^{2+}–S100B). **(a)** Stereo view representation of the backbone superposition (N, Cα and C′ atoms) of the 20 low-energy structures of Ca^{2+}–S100B; the two S100β subunits are shown in green and magenta. The superposition was performed using residues found in the regular secondary structure of each subunit (residues 2–17, 26–28, 30–39, 52–58 and 67–87). Relative to the energy-minimized average structure, the regular secondary structure has a rmsd of 0.68 ± 0.11 Å for the backbone atoms and 1.36 ± 0.11 Å for heavy atoms; the rmsds for the entire backbone and all heavy atoms are 1.35 ± 0.17 Å and 2.18 ± 022 Å, respectively. **(b)** Stereo view representation of the backbone superposition of the 20 low-energy structures of Ca^{2+}–S100B as in (a) but rotated 90° about the assembly x axis. **(c)** Ribbon diagram of Ca^{2+}–S100B illustrating the symmetry between the two S100β subunits. The helices for each subunit are numbered I, II, III and IV (green) and I′, II′, III′ and IV′ (magenta). Although noncrystallographic symmetry was not imposed the rmsd between the two monomers is excellent (rmsd of 0.68 Å for all backbone residues). **(d)** The same figure as in (c) but rotated 90° about the x axis.

differences to that observed for most EF-hand calcium-binding proteins containing isolated two-site domains. The helical arrangement in Ca^{2+}–S100B is most consistent with a bicornate-type of helix packing [53], having only one possible antiparallel helix pair (III, IV). Visual inspection of the monomeric fold, however, suggests a splayed helix relationship more akin to the arrangement found in calbindin D_{9k} [21]. This four-helix packing arrangement is most similar to that of the calcium-bound form of recoverin [13,14] involving helices B and C from calcium-binding site I and helices D and E from site II, although in this case the S100β interhelical angles involving helix I are more obtuse. Furthermore, the interhelical angle for site I in Ca^{2+}–S100β (138°) is in agreement with that observed in other S100 proteins having a characteristic ψ EF-hand.

Table 2

Interhelical angles* in apo calcyclin, apo S100B, Ca^{2+}–S100B and Ca^{2+}–calbindin.

Helices	Apo calcyclin†	Rat apo S100B‡	Bovine apo S100B§	Ca^{2+}–S100B#	Apo calbindin¶	Ca^{2+}–calbindin¥
I–II	140 ± 15	133 ± 3	127 ± 4	138 ± 4	120 ± 3	130 ± 2
I–III	−87 ± 21	−29 ± 2	−66 ± 5	−86 ± 4	−114 ± 8	−114 ± 6
I–IV	118 ± 18	121 ± 2	115 ± 3	113 ± 2	122 ± 3	128 ± 4
II–III	131 ± 13	−139 ± 4	142 ± 5	133 ± 4	121 ± 6	108 ± 5
II–IV	−26 ± 9	−35 ± 2	−45 ± 4	−46 ± 2	−36 ± 4	−33 ± 3
III–IV	149 ± 12	−146 ± 3	169 ± 6	148 ± 4	121 ± 7	118 ± 7

*Calculated using in-house program (S Gagne, University of Alberta). †[40], PDB accession code 1CNP; helices were defined as residues 4–16, 32–42, 53–62 and 70–85. ‡[38], PDB accession code 1SYM; helices were defined as residues 2–17, 30–39, 51–57 and 70–82. §[39], PDB accession code 1CFP; helices were defined as for rat apo S100B. #PDB accession code 1UWO; helices were defined as for rat apo S100B. ¶[20], PDB accession code 1CLB; helices were defined as residues 3–13, 25–35, 46–54 and 63–72. ¥[21], PDB accession code 2BCB; helices were defined as for apo calbindin.

The two S100β monomers pack in an antiparallel fashion about helices IV and IV′ to form the symmetric Ca^{2+}–S100B dimer with overall dimensions of 54 Å × 51 Å × 41 Å (Figures 1c and 1d). This dimeric structure is stabilized primarily by hydrophobic sidechain interactions which result in the burial of ~1170 $Å^2$ of the solvent-accessible surface of each monomer. This value is similar to that observed in apo S100A6 [40] and corroborates findings that a tight association of monomers has been observed for both apo [54] and Ca^{2+}–S100B. The dimer interface primarily involves hydrophobic interactions between helices I and I′ and helices IV and IV′. Contacts between helices I and I′ extend nearly the entire length of each helix (Glu2–Val13). The identification of the interactions between helices I and I′ was confirmed by important sidechain NOEs observed between residues Leu3–Leu10′ and Ala6–Ala9′. These contacts were clearly indicative of intermonomer contacts at the dimer interface as this type of interaction is not possible within a single helix.

The vast majority of EF-hand calcium-binding proteins comprise isolated pairs of EF-hands. A much smaller number, including S100B and recoverin, comprise clusters of two-site pairs of EF-hands and allow an examination of the helix orientation at this interface. In Ca^{2+}–S100B, helices I and I′ cross at an angle of 142° ± 3°, which is more open than compared to the helix I–I′ packing in apo S100B (161° and 151° for rat [38] and bovine [39], respectively). The crossing point of these helices, involving residues Ala6 and Ala9, is consistent with small hydrophobic residues being favored at these positions. Helices IV and IV′ form a more obtuse interhelical angle (155° ± 2°) making contacts similar to those found in apo S100B between residues at the N-terminal (Phe70) and more C-terminal regions (Thr82′) of the helices. Overall, this arrangement can be catalogued as an 'X bundle' [53] in both Ca^{2+}–S100B and apo S100B [38,39]. This helical arrangement is also present at the crystallographic dimer interface of sarcoplasmic calcium-binding protein [55], where helices C and E form an antiparallel pair roughly perpendicular to their symmetrically related helices in the dimer molecule. Furthermore, the interface for sites I–II and III–IV in apo recoverin [15] also display similar features, including an antiparallel alignment of helices E and F between sites II and III and a perpendicular arrangement of these helices to helix G in site III. In recoverin, however, a parallel partner to helix G is absent.

Helix IV is elongated in human Ca^{2+}–S100B with respect to rat and bovine apo S100B [38,39] and apo S100A6 [40], but is bent by approximately 7° near residue Ala83. The impact of this lengthening in Ca^{2+}–S100B is to absolve the dimer interface of Phe87 and Phe88 in the Ca^{2+}–S100B structure. These residues have been suggested to be integral to dimer maintenance in apo S100 proteins and are largely buried in the apo S100A6 [40] (Leu88) and apo S100B [38,39] (Phe87–Phe88) structures. While the removal of these residues could act to destabilize the S100 dimer, we have observed that S100B remains dimeric and of similar stability both in the absence and presence of calcium when Phe88 is conservatively replaced with an alanine residue (KL Harper and GSS, unpublished results).

The helical content was calculated for Ca^{2+}–S100B and for the NMR structures of apo rat [38] and bovine S100B [39] from the ratio of helical residues, based on the structures, to the total number of residues in the protein (91 amino acids/monomer). This comparison shows human Ca^{2+}–S100B contains 57% α helix which is similar to that observed in rat apo S100B (60%) [38] but somewhat smaller than that observed in bovine apo S100B (66%) [39]. In human Ca^{2+}–S100B an α helix is not observed at residues Ser41–Glu45 in the linker; a short α helix is observed in this position in bovine apo S100B [39]. Despite our observation of some lengthening of helix IV, the negligible change or slight decrease in α-helicity in human Ca^{2+}–S100B compared to bovine apo S100B [39] is consistent with previous circular dichroism (CD) studies

[41], which indicated calcium binding resulted in a 10% decrease in θ_{222}.

Calcium-induced conformational changes

The response to calcium binding by S100B is best assessed by comparing the conformations of the two calcium-binding sites in the apo and Ca^{2+}–S100B structures. The N-terminal helix-loop-helix in Ca^{2+}–S100B (residues Val8–Glu39) is very similar in form to that of apo rat S100B [38], having a backbone pairwise rmsd ~1.40 Å (Figure 2a). This observation indicates that a large alteration in the conformation of this calcium-binding loop has not occurred. Interhelical angles of 138°, for site I helices in Ca^{2+}–S100B, and 133° for the same site in rat apo S100B [38] confirm that there is little reorientation of the helices upon calcium binding (Table 2). This observation is consistent with that seen in calbindin D_{9k} where structures of apo [20] and calcium-bound [21] forms of the protein have site I interhelical angles of 120° and 130°, respectively. As a result, the site I calcium-binding loop in Ca^{2+}–S100B is also similar to the structure observed in Ca^{2+}–calbindin D_{9k} [21] (backbone pairwise rmsd ~1.06 Å; Figure 2a). Detailed comparisons of apo and Ca^{2+}–calbindin D_{9k} indicate that changes which occur in the N-terminal ψ EF-hand primarily entail the reorganization of sidechains upon calcium binding [20,21,56].

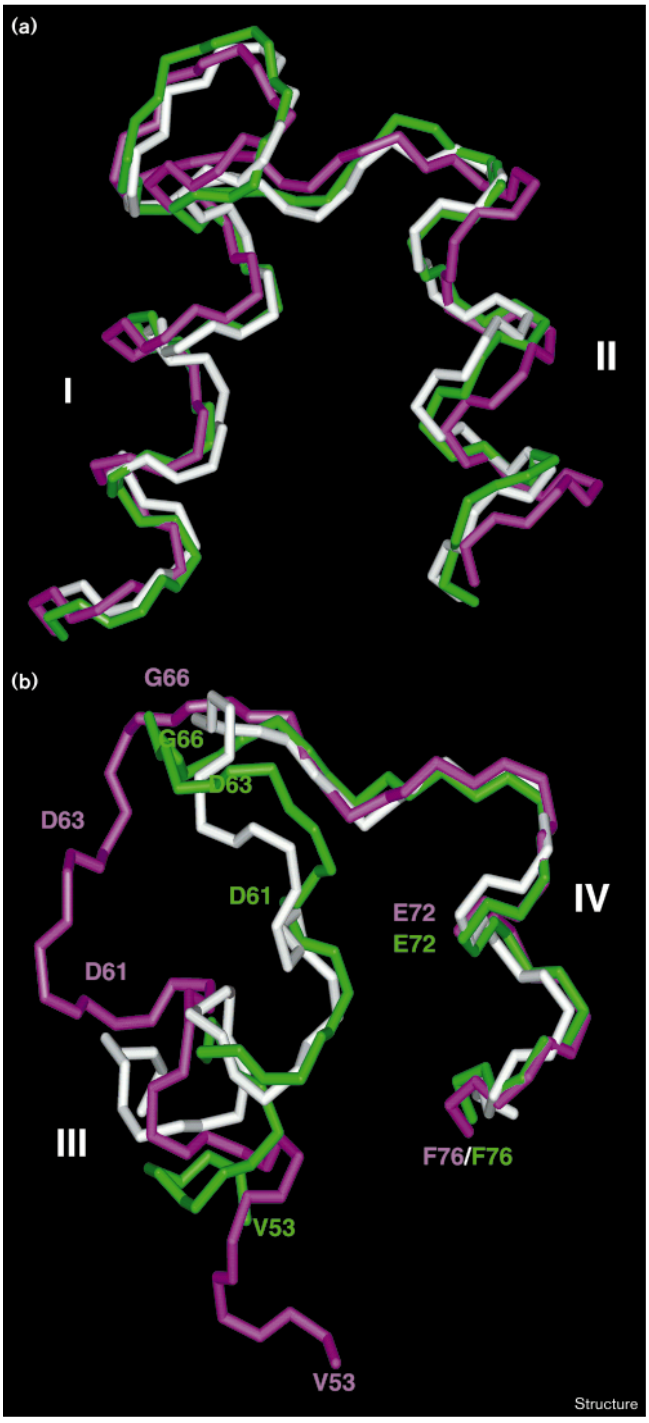

The C-terminal EF-hand in S100B has a high degree of sequence similarity to other EF-hand calcium-binding sites [57], and includes a 12-residue loop possessing acidic residues required for calcium coordination at four positions: Asp61 (X), Asp63 (Y) and Asp65 (Z) and Glu72 (–Z). The structure of Ca^{2+}–S100B reveals that this loop (Figure 2b) adopts a conformation similar to that observed for the calcium-filled sites in classical EF-hand proteins, such as calmodulin (backbone pairwise rmsd ~1.59 ± 0.08 Å, for four calcium-binding loops [6]) and troponin C (backbone pairwise rmsd ~1.12 ± 0.18 Å for the two C-terminal EF-hand motifs [58]). The average ϕ,ψ angles for Ca^{2+}–S100B for Asp61 (–70° ± 16°,101° ± 12°), Glu72 (–78° ± 3°,–24° ± 9°) and the invariant Gly66 (73° ± 5°,18° ± 13°) between the Z (Asp65) and –Y (Glu67) coordinating positions are in agreement with consensus values for these backbone angles in EF-hand

Figure 2

Comparison of the EF-hands of human Ca^{2+}–S100B, rat apo S100B [38] and Ca^{2+}–calbindin D_{9k} [21]. **(a)** The N-terminal pseudo EF-hand in Ca^{2+}–S100B (green) and rat apo S100B [38] (magenta), superimposed (N, Cα and C′atoms) with the analogous residues in the pseudo EF-hand of Ca^{2+}–calbindin D_{9k} [21] (white). The three helix-loop-helix motifs, comprised of incoming helix I, outgoing helix II and the intervening calcium-binding loop, have similar folds. The structures have a backbone pairwise rmsd of 1.40 Å for apo S100B [38] and Ca^{2+}–S100B (residues Val8–Glu39) and 1.06 Å for Ca^{2+}–calbindin D_{9k} [21] (residues Glu4–Glu35) and Ca^{2+}–S100B (residues Val8–Glu39). **(b)** The superposition (N, Cα and C′atoms) of the C-terminal EF-hands of Ca^{2+}–S100B (green) and rat apo S100B [38] (magenta) with the analogous residues of Ca^{2+}–calbindin D_{9k} [21] (white). The mainchain atoms of the β sheet and a portion of helix IV were superimposed yielding an rmsd of 0.55 Å for apo S100B [38] and Ca^{2+}–S100B (residues Glu67–Phe76) and 0.95 Å for Ca^{2+}–calbindin D_{9k} [21] (residues Glu60–Leu69) and Ca^{2+}–S100B (residues Glu67–Phe76). Superposition of the entire EF-hand backbone of rat apo S100B [38] relative to Ca^{2+}–S100B (residues Val53–Phe76) yielded an rmsd of 4.06 Å compared to 1.47 Å for Ca^{2+}–calbindin D_{9k} [21] (Leu46–Leu69).

calcium-binding proteins [59]. The ϕ,ψ angles for Asp63 and Asp65 deviate slightly from those expected for a classical EF-hand. This deviation is likely to be due to the intervening glycine (Gly64). The ϕ,ψ angles for Gly64 are, however, similar to those observed in calbindin D_{9k} [21] (Figure 2b).

The C-terminal calcium-binding loop in S100B undergoes a dramatic change in conformation compared to that of rat apo S100B [38]. This change is illustrated in Figure 2b, where the C-terminal portion of the calcium-binding loop and helix IV (Glu67–Phe76) for human Ca^{2+}–S100B, rat apo S100B [38] and Ca^{2+}–calbindin D_{9k} [21] are superimposed. In this presentation it is clear that the relative orientations of the β sheet and helix IV are maintained in Ca^{2+}–S100B compared to both rat apo S100B [38] (backbone pairwise rmsd ~0.55 Å) and Ca^{2+}–calbindin D_{9k} [21] (backbone pairwise rmsd ~0.95 Å). Similar observations were also made for the same region in bovine apo S100B [39] (backbone pairwise rmsd ~0.63 Å) and apo S100A6 [40] (backbone pairwise rmsd ~0.74 Å) when compared to human Ca^{2+}–S100B. However, a comparison of the entire calcium-binding loop (Asp61–Glu72) and the same region of helix IV (Phe73–Phe76) between Ca^{2+}–S100B and rat apo S100B [38] reveals a more significant difference (rmsd ~4.06 Å). The cause for this difference can be traced to the first six residues of the calcium-binding loop. More specifically, changes in the ϕ,ψ angles of Asp61 (30°,169°) and Asp63 (62°,16°) and a ψ angle change from –142° to 12° for Gly66 upon calcium binding lead to a rearrangement of the C-terminal loop in Ca^{2+}–S100B bringing the sidechains of Asp61 and Asp63 into a more appropriate geometry to coordinate calcium.

The change in conformation of the C-terminal loop in human S100B upon calcium binding is propagated through helix III, which immediately precedes the loop. This results in a major reorientation of helix III, with respect to helices II and IV, yielding changes in the respective interhelical angles of about 90° and 66° compared to rat apo S100B [38] (Table 2). The net impact of this reorientation is to change the 'handedness' of the II–III and III–IV interhelical crossings from negative to positive interhelical angles (Table 2). The movement of helix III relative to helices II and IV results in large changes in the surface area accessibility of several residues in the linker and helices III and IV compared to rat apo S100B [38] (Figure 3). One possible consequence of this is a relative increase in amide exchange in helix III compared to residues in the other helices [49], although interpretation of this observation cannot be made until exchange rate information is available. The change in relationship between helices II, III and IV has a significant impact on the helix I–III angle which opens by nearly 60° upon calcium binding.

Support for a biological switch

It has been proposed that the linker region and C terminus of S100B may be important for calcium-sensitive surface interactions with target proteins, such as neuromodulin, GFAP and tubulin [16]. The surface of Ca^{2+}–S100B takes on a bilobal appearance revealing a deep negatively charged cleft first observed in apo S100A6 [40] and bordered by helices III, III′, IV and IV′ (Figure 1d). Examination of this surface and comparison to the rat apo S100B protein structure was used to determine changes in the accessible surface area of discrete residues (Figure 3). It is clear that calcium binding and the reorientation of helix III has resulted in increases and decreases in the accessible surface area of many residues, particularly in the C terminus of the protein. As expected, calcium binding results in a decrease in exposure of residues Asp61, Glu67 and, Glu72 in the C-terminal calcium-binding loop, in agreement with the large conformational change observed (Figure 2b). Smaller changes are observed in the ψ EF-hand but notably Lys29 becomes more exposed in a similar manner to that observed for calbindin D_{9k} [20,21]. Overall calcium binding to S100B results in an average increase of 420 $Å^2$ of surface area in the dimer.

Upon calcium binding it has been previously noted that S100B takes on a more hydrophobic characteristic, as is evident from its increased affinity to phenyl sepharose [60] and aggregation in solution [42]. Correspondingly, greater than 90% of the newly exposed surface area in Ca^{2+}–S100B is hydrophobic in nature. Most notable are the hydrophobic residues Phe43 in the linker region and Ala83, Phe87 and Phe88 of the C-terminal helix which are in close proximity to one another in each S100β subunit (Figure 4). This observation is supported by spectrophotometric results which show that at least one phenylalanine residue is exposed upon calcium binding [41,42,61]. Furthermore, several acidic residues, including Glu49 and Asp54, experience greater exposure to solvent while Glu45, Glu46, and Glu51 remain solvent-exposed (Figures 3a and 4). Interestingly, the exposure of the hydrophobic and acidic residues, including residues in the linker and the C-terminal of helix IV, is tantalizingly similar to that observed in calmodulin [6]. Reinforcing these results are observations that S100B displays a calcium-sensitive interaction with short peptides, isolated from a bacterial random peptide display library, comprised mainly of basic and hydrophobic residues [62] in a fashion reminiscent of MLCK and the autoregulatory region of twitchin kinase, the S100A1 target [25]. This observation indicates that Phe43, Phe87, Phe88, Glu45, Glu46, Glu49 and Glu51 are prime candidate residues for making a calcium-sensitive interaction with a protein target (Figure 4). Acidic residues at the extreme C terminus (Glu86,Glu89 and Glu91) are also exposed and may be important, however, Glu89 and Glu91 are poorly defined

Figure 3

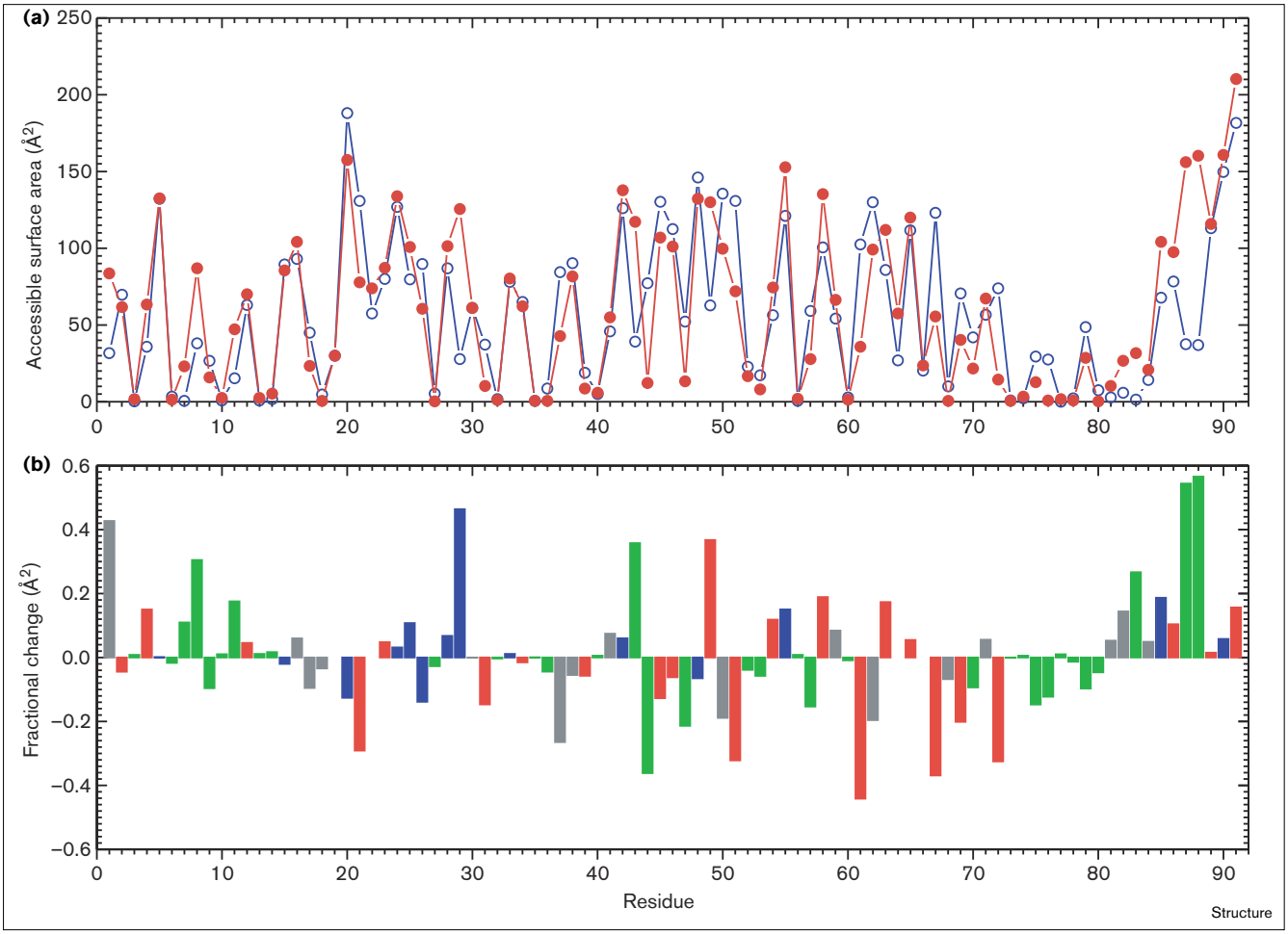

Accessible surface area for S100B. **(a)** Accessible surface area per residue for rat apo S100B (blue) [38] and human Ca^{2+}–S100B (red) determined from 20 structures of each. The values shown are the averages from both monomers (generally < 10% difference). Surface areas were defined using a probe having a 1.4 Å radius [64] using the solvation module of InsightII (Biosym Technologies). **(b)** Fractional surface area changes between rat apo S100B and human Ca^{2+}–S100B determined from the measured difference in (a) divided by the per residue surface area. Positive bars denote increased exposure in Ca^{2+}–S100B. Bars are color-coded by residue type: basic (blue), acidic (red), hydrophobic (green) and others (grey).

in the Ca^{2+}–S100B structure. Other evidence supports the potential role of the C-terminal hydrophobic residues. For example, site-directed mutagenesis of the S100 family member S100A10 indicated that residues Phe85 and Phe86 (Phe87 and Phe88 in S100B) are critical for its interaction with annexin II, implying these residues are exposed [63].

While S100B is suggested to be a calcium-sensitive modulatory protein, similar to troponin C, calmodulin and recoverin, S100B also possesses the unique quality of high-affinity zinc binding. The calcium affinity of several S100 family members, including S100B [23,60], S100A3 [64] and S100A12 (calgranulin C) [65], is enhanced in the presence of zinc. Furthermore, zinc binding to S100A1 results in a 30-fold lowering of the concentration of S100A1 required for calcium–S100A1-dependent activation of twitchin kinase [25]. Although sequence analysis reveals several S100 protein family members to contain a number of histidine and cysteine residues capable of chelating zinc, it has not been possible to propose a possible zinc-binding site in S100B. The Ca^{2+}–S100B structure reveals several histidine residues at the S100B dimer interface which are clustered together. Specifically, the sidechains of His15 and His25 are closely spaced (~5 Å) while the sidechain of His85 from the symmetric subunit is also nearby (~9 Å). A fourth potential zinc ligand may arise from His90 (~8 Å from His25) which lies outside helix IV and in the flexible (unstructured) C terminus of S100B. It would seem that a very small reorientation

Figure 4

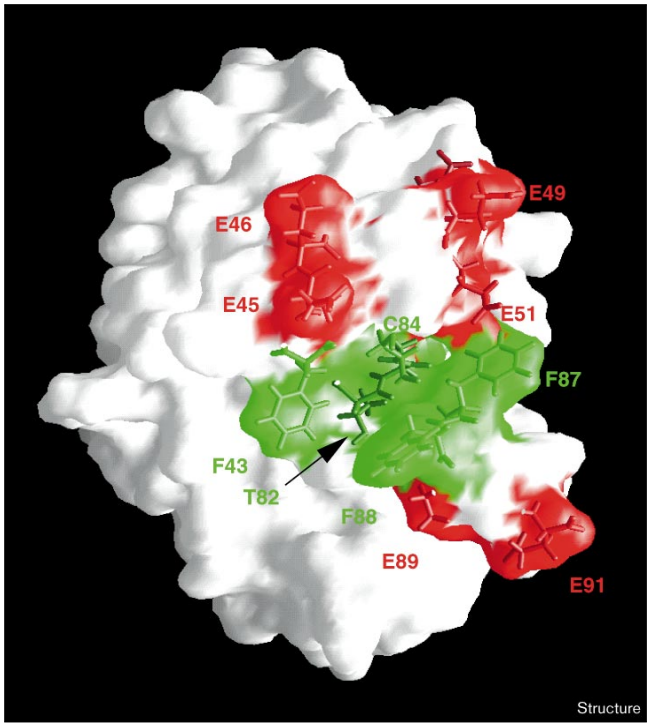

A portion of the proposed target protein recognition site in human S100B. Exposed residues and those observed to have increased exposure in Ca^{2+}–S100B as compared to apo S100B (Figure 3) are superimposed on the molecular surface of Ca^{2+}–S100B. The molecule is oriented with helix IV in front. Exposed aromatic residues Phe43, Phe87 and Phe88 and aliphatic residues Thr82, Ala83 (not labeled) and Cys84 are shown in green. Acidic residues Glu45, Glu46, Glu49, Glu51, Glu89 and Glu91 are shown in red. (Figure was generated using the program GRASP [86].)

would bring all four sidechains into position to coordinate zinc. An attractive feature of this model is that it corroborates work by Donato *et al.* [66] suggesting zinc binds to a region including His15 and His25.

Extracellular roles have been proposed for S100B based on the observation that covalent, disulfide-linked forms of the protein have been shown to possess neurotrophic activity [67,68]. Interestingly, the formation of these disulfide-linked dimers is calcium-sensitive and temperature-sensitive [69]. The Ca^{2+}–S100B structure indicates that the exposure of Cys84 could provide an explanation for the formation of the disulfide species. However, examination of Cys84 with respect to its symmetrically related residue and either Cys68 or Cys68′ indicates no clear relationship for the formation of an oxidized species. The symmetrically related Cys84′ is remotely located (31 Å) from this site and both Cys68 and Cys68′, although not accessible are further removed (19 Å and 18 Å, respectively). It is possible that oxidation may result in the formation of a higher order species, as observed in the calcium-sensitive formation of tetrameric (and higher) S100A8 and S100A9 complexes [70]. Clearly this remains to be established, as does the mechanism by which S100B is secreted.

Biological implications

S100B is a member of the dimeric S100 protein family of EF-hand calcium-binding proteins and has been proposed to play a role in cell growth and differentiation as well as in cytoskeletal structure and function. Several target proteins have been identified which all exhibit a calcium-dependent requirement for interaction with S100B. The three-dimensional structures of rat and bovine S100B [38,39] and S100A6 [40] in the calcium-free state have recently been determined. Nevertheless, in order to further understand the mechanisms underlying S100 protein intracellular signalling it will be necessary to establish the molecular details behind a calcium-induced conformational change in S100B that is required for target recognition. We present here the solution structure of human S100B in the calcium-bound state; the structure reveals a novel calcium switch that may be used for target recognition.

The S100B monomer is a single globular domain containing two EF-hand calcium-binding sites, termed site I and site II. Calcium binding to S100B causes little change in the conformation of calcium-binding site I, as it takes on a 'calcium-ready' conformation observed in the apo state [38]. In the site II calcium-binding loop, however, a significant reorientation of N-terminal residues occurs allowing for coordination of the calcium ion. This reorientation results in a dramatic change in the position of one of the helices, helix III, relative to the other three helices. This conformational change results in the exposure of hydrophobic residues at the C terminus of helix IV (Ala83, Phe87 and Phe88) and in the linker (Phe43). These two regions, which are the most divergent among the S100 protein family members and have been proposed as key regions for target protein specificity, are close spatially and provide an attractive target-recognition site. While this 'calcium switch' follows the general characteristics of other calcium-dependent modulatory proteins, that is the exposure of a hydrophobic surface, the molecular details behind the exposure are unique from those of troponin C or calmodulin. With the identification of this calcium switch in hand, the molecular details of S100B–target protein complexes can now be pursued to complete the entire S100B calcium activation mechanism.

Materials and methods

Sample preparation

Uniformly ^{15}N- and $^{15}N/^{13}C$-labeled recombinant human S100B was expressed in *Escherichia coli* (strain N99) and purified to homogeneity as previously described [42]. NMR experiments utilized 2–2.5 mM human S100B samples dissolved in 81% H_2O/ 9% D_2O/ 10% TFE-d_3

containing 30 mM KCl, 10 mM DTT-d_{10}, 10 mM $CaCl_2$, 0.1 mM NaN_3 at pH 7.05. A single $^{15}N/^{13}C$-labeled sample was used for all triple resonance NMR experiments.

NMR spectroscopy

All NMR experiments were performed at 35°C on a Varian Unity 500 MHz spectrometer equipped with a triple resonance, pulsed-field gradient (PFG) probe. Sequential assignments of the backbone resonances were achieved via HNCACB [71] and CBCA(CO)NH [72] triple resonance experiments in combination with HNCO [73] and ^1H-^{15}N NOESY-HSQC [74] (τ_{mix} = 50 and 150 ms) experiments as previously reported. Sidechain assignments were obtained from HCCH-TOCSY [75] and simultaneous $^{15}N/^{13}C$-separated three-dimensional (3D) NOESY-HSQC [76] (τ_{mix} = 100 ms) experiments while aromatic proton assignments were made from a 100 ms two-dimensional (2D) homonuclear NOESY [77,78] experiment. NMRPipe and NMRDraw [79] software packages were used to process all data sets and data analysis was carried out with the aid of Pipp and Stapp [80].

Slow-exchanging amide protons were identified via a series of ^1H-^{15}N HSQC [81] experiments taken at time intervals (10 min, 1.5 h, 6 h, and 14 h) after dissolving the protein in D_2O. Backbone coupling constants, $^3J_{NH\alpha}$, were calculated from an HNHA [82,83] experiment as previously described [49]. Stereospecific assignments of valine methyl groups were obtained by analyzing the intraresidue HN/CH_3 and CαH/CH_3 from the ^{15}N-edited NOESY-HSQC and the simultaneous $^{15}N/^{13}C$-separated 3D NOESY-HSQC spectra. Stereospecific assignments were also made for Hβ methylene protons of several AMX residues by analyzing the intensities of intraresidue HN/Hβ and Hα/Hβ from the ^{15}N-edited NOESY-HSQC and the simultaneous $^{15}N/^{13}C$-separated 3D NOESY-HSQC spectra.

Structure determination

Approximate interproton distances were obtained from the 50 ms ^{15}N-separated 3D NOESY-HSQC [74], simultaneous $^{15}N/^{13}C$-separated 3D NOESY-HSQC [76], and homonuclear 2D NOESY experiments [77,78]. NOE cross-peaks identified from the 50 ms ^{15}N-edited NOESY experiment were calibrated for each residue on the basis of the known distances of intraresidue $d_{HN\alpha}$ and sequential $d_{\alpha HN}$ while known aromatic Hδ–Hε distances were used to calibrate NOEs from the aromatic region of the homonuclear 2D NOESY. The 100 ms $^{15}N/^{13}C$-separated 3D NOESY was calibrated to geminal protons or protons on adjacent carbon atoms. In cases where direct calibration was not possible, the distance constraints were overestimated. The calibration was carried out in a similar fashion to that used in the structure calculation of a calcium-saturated skeletal troponin C mutant [84]. Upper and lower bounds for distance restraints derived solely from NOEs identified in the 150 ms ^{15}N-NOESY-HSQC experiment and not observed in the 50 ms experiment were automatically set to 6.00 Å and 1.70 Å, respectively. Dihedral restraints for ϕ angles were derived from the $^3J_{HN\alpha}$ coupling constants, and the ψ angles were obtained from the $d_{N\alpha}/d_{\alpha N}$ ratio as previously described [49]. For the ϕ and ψ angles, values of $-60° \pm 30°$ and $-40° \pm 30°$ were used for helical regions and values of $-120° \pm 50°$ and $120° \pm 50°$ were used for β strands. Hydrogen bond restraints were identified from slowly exchanging NH resonances and were implemented only after their identification in initial structures. Two distance restraints, r_{NH-O} (1.8–2.3 Å) and r_{N-O} (2.3–3.3 Å), were used for each hydrogen bond.

Initial structures of the Ca^{2+}–S100B monomer were calculated using the hybrid distance geometry and simulated-annealing protocol in the program X-PLOR 3.1 [85]. A series of refinements were carried out using the simulated annealing refinement protocol incorporating ϕ and ψ angles as well as hydrogen-bond restraints. A family of 30 low-energy Ca^{2+}–S100β monomer structures were generated based on 1118 interproton distances (570 intraresidue, 264 sequential, 209 short range, and 75 long range), 68 distance restraints for 34 hydrogen bonds, and 115 dihedral angle restraints. No distance violations $>$ 0.3 Å and no dihedral violations $>$ 5° were found for this family of structures.

Structure determination of the Ca^{2+}–S100B dimer involved the duplication of the coordinates for each of the 30 low-energy subunit structures. Each new subunit was rotated 180° and separated from its partner by approximately 40 Å. No docking of the two monomers was attempted or used prior to further structure calculations. Final dimer structures were calculated using the hybrid distance geometry, simulated annealing, and simulated annealing refinement protocols of X-PLOR 3.1 [85]. These procedures utilized all 2236 intramolecular NOE-derived distance restraints, 230 dihedral angles, 68 hydrogen-bond restraints, and 40 unambiguous intermolecular distance restraints. This approach led to 20 low-energy Ca^{2+}–S100B dimer structures having no NOE violations $>$ 0.5 Å, no dihedral violations $>$ 5°, and low rmsds compared to an average structure. NCS or distance symmetry was not imposed at any point in the dimer structure calculations. Calcium ions or restraints to these ions were not used in any structure calculations.

Accession numbers

Atomic coordinates have been deposited with the Protein Data Bank, Brookhaven National Laboratories, with the accession code 1UWO for the ensemble of 20 Ca^{2+}–S100B structures.

Acknowledgements

We thank Kathryn Barber (University of Western Ontario) for her technical support and Lewis Kay (University of Toronto) for advice and providing all pulse sequences. We are grateful to Frank Delaglio and Dan Garrett (NIH) for NMRPipe and Pipp. We also thank Stéphane Gagne (University of Alberta) for providing structure analysis programs and many useful discussions. This research was supported by operating and maintenance grants from the Medical Research Council of Canada (GSS) and an Alzheimer Society of Canada Doctoral Award (SPS). Funding for the NMR spectrometer in the McLaughlin Macromolecular Structure Facility was made possible through grants from the Medical Research Council of Canada and the Academic Development Fund of the University of Western Ontario and generous gifts from the R Samuel McLaughlin Foundation and the London Life Insurance Company of Canada. This work was presented at the 11th Symposium of the Protein Society, July 12–16, 1997.

References

1. Kretsinger, R.H. & Nockolds, C.E. (1973). Carp muscle calcium-binding protein. II. Structure determination and general description. *J. Biol. Chem.* **248**, 3313–3326.
2. Ikura, M. (1996). Calcium binding and conformational response in EF-hand proteins. *Trends Biochem.* Sci. **21**, 14–17.
3. Gagné, S.M., Tsuda, S., Li, M.X., Chandra, M., Smillie, L.B. & Sykes, B.D. (1994). Quantification of the calcium-induced secondary structural changes in the regulatory domain of troponin-C. *Protein Sci.* **3**, 1961–1974.
4. Gagné, S.M., Tsuda, S., Li, M.X., Smillie, L.B. & Sykes, B.D. (1995). Structures of the troponin C regulatory domains in the apo and calcium-saturated states. *Nat. Struct. Biol.* **2**, 784–789.
5. Finn, B.E., Evenäs, J., Drakenberg, T., Walthro, J.P., Thulin, E. & Forsén, S. (1995). Calcium-induced structural changes and domain autonomy in calmodulin. *Nat. Struct. Biol.* **2**, 777–783.
6. Ikura, M., Clore, G.M., Gronenborn, A.M., Zhu, G., Klee, C.B. & Bax, A. (1992). Solution structure of a calmodulin–target peptide complex by multidimensional NMR. *Science* **256**, 632–638.
7. Kuboniwa, H., Tjandra, N., Grzesiek, S., Ren, H., Klee, C.B. & Bax, A. (1995). Solution structure of calcium-free calmodulin. *Nat. Struct. Biol.* **2**, 768–776.
8. Zhang, M. Tanaka, T. & Ikura, M. (1995). Calcium-induced conformational transition revealed by the solution structure of apo calmodulin. *Nat. Struct. Biol.* **2**, 758–767.
9. Zhang, M., Li, M., Wang, J. & Vogel, H.J. (1994). The effect of Met-Leu mutations on calmodulin's ability to activate cyclic nucleotide phosphodiesterase. *J. Biol. Chem.* **269**, 15546–15552.
10. Yuan, T., Mietzner, T.A., Montelaro, R.C. & Vogel, H.J. (1995). Characterization of the calmodulin binding domain of SIV transmembrane glycoprotein by NMR and CD spectroscopy. *Biochemistry* **36**, 10690–10696.
11. Siivari, K., Zhang, M., Palmer,. A.G., III. & Vogel, H.J. (1995). NMR studies of the methionine methyl groups in calmodulin. *FEBS Lett.* **366**, 104–108.

12. Ames, J.B., Tanaka, T., Stryer, L. & Ikura, M. (1996). Portrait of a myristoyl switch protein. *Curr. Opin. Struct. Biol.* **6**, 432–438.
13. Ames, J.B., Ishima, R., Tanaka, T., Gordon, J.I., Stryer, L. & Ikura, M. (1997). Molecular mechanics of calcium-myristol switches. *Nature* **389**, 198–202.
14. Flaherty, K.M., Zozulya, S., Stryer, L. & McKay, D.B. (1993). Three-dimensional structure of recoverin, a calcium sensor. *Cell* **75**, 709–716.
15. Tanaka, T., Ames, J.B., Harvey, T.S., Stryer, L. & Ikura, M. (1995). Sequestration of the membrane-targeting myristoyl group of recoverin in the Ca^{2+}-free state. *Nature* **376**, 444–447.
16. Hilt, D.C. & Kligman, D. (1991). The S-100 protein family: a biochemical and functional overview. In *Novel Calcium-Binding Proteins. Fundamentals and Clinical Implications.* (Heinzmann, C.W., ed.), pp. 65–103, Springer-Verlag, Berlin.
17. Fanò, G., Biocca, S., Fulle, S., Mariggiò, M., Belia, S. & Calissano, P. (1995). The S100: a protein family in search of a function. *Prog. Neurobiol.* **46**, 71–82.
18. Zimmer, D.B., Cornwall, E.H., Landar, A. & Song, W. (1995). The S100 protein family: history, function, and expression. *Brain Res. Bulletin.* **37**, 417–429.
19. Schäfer, B.W. & Heizmann, C.W. (1996). The S100 family of EF-hand calcium-binding proteins: functions and pathology. *Trends Biochem. Sci.* **21**, 134–140.
20. Skelton, N.J., Kördel, J. & Chazin, W.J. (1995). Determination of the solution structure of apo calbindin D_{9k} by NMR spectroscopy. *J. Mol. Biol.* **249**, 441–462.
21. Kördel, J., Skelton, N.J., Akke, M. & Chazin, W.J. (1993). High resolution solution structure of calcium-loaded calbindin D_{9k}. *J. Mol. Biol.* **231**, 711–734.
22. Kligman, D. & Hilt, D.C. (1988). The S100 protein family. *Trends Biochem. Sci.* **13**, 437–443.
23. Baudier, J., Glasser, N., Haglid, K., & Gerard, D. (1984). Purification, characterization and ion binding properties of human brain S100b protein. *Biochem. Biophys. Acta.* **790**, 164–173.
24. Baudier, J., Glasser, N. & Gerard, D. (1986). Ions binding to S100 proteins. I. Calcium and zinc binding properties of bovine brain S100αα, S100a (αβ) and S100b (ββ) protein: Zn^{2+} regulates Ca^{2+} binding to S100b protein. *J. Biol. Chem.* **261**, 8192–8203.
25. Heierhorst, J., *et al*., & Kemp, B.E. (1996). Ca^{2+}/S100 regulation of giant protein kinases. *Nature* **380**, 636–639.
26. Van Eldik, L.J. & Zimmer, D.B. (1987). Secretion of S-100 from rat C6 glioma cells. *Brain Res.* **436**, 367–370.
27. Marshak, D.R., Pesce, S.A., Stanley, L.C. & Griffin, W.S.T. (1991). Increased S100β neurotrophic activity in Alzheimer's disease temporal lobe. *Neurobiol. Aging.* **13**, 1–7.
28. Van Eldik, L.J. & Griffin, W.S.T. (1994). S100β expression in Alzheimer's disease: relation to neuropathology in brain regions. *Biochim. Biophys. Acta.* **1223**, 398–403.
29. Griffin, W.S.T., *et al*., & Araoz, C. (1989). Brain interleukin 1 and S100 immunoreactivity are elevated in Down syndrome and Alzheimer disease. *Proc. Natl. Acad. Sci.* **86**, 7611–7615.
30. Donato. R. (1988). Calcium-independent, pH-regulated effects of S-100 proteins on assembly-disassembly of brain microtubule protein *in vitro*. *J. Biol. Chem.* **263**, 106–110.
31. Donato, R., Giambanco, I. & Aisa, M.C. (1989). Molecular interaction of S-100 proteins with microtubule proteins *in vitro*. *J. Neurochem.* **53**, 566–571.
32. Bianchi, R., Giambanco, I. & Donato, R. (1993). S-100 protein but not calmodulin binds to the glial fibrillary acid protein and inhibits its polymerization in a Ca^{2+}-dependent manner. *J. Biol. Chem.* **268**, 12669–12674.
33. Sheu, F.-S., Azmitia, E.C., Marshak, D.R., Parker, P.J. & Routtenberg, A. (1994). Glial-derived S100β protein selectively inhibits recombinant β protein kinase C (PKC) phosphorylation of neuron-specific protein F1/GAP43. *Mol. Brain Res.* **21**, 62–66.
34. Sheu, F.-S., Huang, F.L. & Huang, K.-P. (1995). Differential responses of protein kinase C substrates (MARCKS, neuromodulin and neurogranin) phosphorylation to calmodulin and S100. *Arch. Biochem. Biophys.* **316**, 335–342.
35. Lin, L.-H., Van Eldik, L.J., Osheroff, N. & Norden, J.J. (1994). Inhibition of protein kinase C- and casein kinase II-mediated phosphorylation of GAP-43 by S100β. *Mol. Brain Res.* **25**, 297–304.
36. Baudier, J., Mochly-Rosen, D., Newton, A., Lee, S.-H., Koshland, D.E. & Cole, R.D. (1987). Comparison of S100β with calmodulin: interactions of melittin and microtubule-associated proteins and inhibition of phosphorylation of τ proteins by protein kinase C. *Biochemistry* **26**, 2886–2893.
37. Baudier, J. & Cole, R.D. (1988). Interactions between the microtubule-associated τ proteins and S100β regulate τ protein phosphorylation by the Ca^{2+}-calmodulin-dependent protein kinase II. *J. Biol. Chem.* **263**, 5876–5883.
38. Drohat, A.C., Amburgey, J.C., Abildgaard, F., Starich, M.R., Baldisseri, D. & Weber, D.J. (1996). Solution structure of rat apo-S100B (ββ) as determined by NMR spectroscopy. *Biochemistry* **35**, 11577–11588.
39. Kilby, P.M. Van Eldik, L.J., & Roberts, G.C.K. (1996). The solution structure of the bovine S100B dimer in the calcium-free state. *Structure* **4**, 1041–1052.
40. Potts, B.C.M., *et al.,* & Chazin, W.J. (1995). The structure of calcyclin reveals a novel homodimeric fold for S100 Ca^{2+}-binding proteins. *Nat. Struct. Biol.* **2**, 790–796.
41. Mani, R.S., Shelling, J.G., Sykes, B.D. & Kay, C.M. (1983). Spectral studies on the calcium binding properties of bovine brain S-100b protein. *Biochemistry* **22**, 1734–1740.
42. Smith, S.P., Barber, K.R., Dunn, S.D. & Shaw, G.S. (1996). Structural influence of cation binding to recombinant human brain S100b: evidence for calcium-induced exposure of a hydrophobic surface. *Biochemistry* **35**, 8805–8814.
43. Baudier, J. & Gerard, D. (1986). Ions binding to S100 proteins. II. Conformational studies and calcium-induced conformational changes in S100αα protein: the effect of acidic pH and calcium incubation on subunit exchange in S100a (αβ) protein. *J. Biol. Chem.* **261**, 8402–8212.
44. Baudier, J. & Gerard, D. (1983). Ions binding to S100 proteins: structural changes induced by calcium and zinc on S100a and S100b proteins. *Biochemistry* **22**, 3360–3369.
45. Mani, R.J., Boyes, B.E. & Kay, C.M. (1982). Physiochemical and optical studies on calcium- and potassium-induced conformational changes in bovine brain S-100β protein. *Biochemistry* **21**, 2607–2612.
46. Slupsky, C.M., Kay, C.M., Reinach, F.C., Smillie, L.B. & Sykes, B.D. (1995). Calcium-induced dimerization of troponin C: mode of interaction and use of trifluoroethanol as a denaturant of quaternary structure. *Biochemistry* **34**, 7365–7375.
47. Anglister, J., Grzesiek, S., Ren, H., Klee, C.B. & Bax, A. (1994). Isotope-edited multidimensional NMR of calcineurin B in the presence of the non-deuterated detergent CHAPS. *J. Biomol. NMR* **3**, 121–126.
48. Slupsky, C.M. & Sykes, B.D. (1995). The NMR solution structure of calcium-saturated skeletal muscle troponin-C. *Biochemistry* **34**, 15953–15964.
49. Smith, S.P. & Shaw, G.S. (1997). Assignment and secondary structure of calcium-bound human S100B. *J. Biomol. NMR* **10**, 77–88.
50. Smith, S.P., Barber, K.R. & Shaw, G.S. (1997). Identification and structural influence of a differentially modified N-terminal methionine in human S100b. *Protein Sci.* **6**, 1110–1113.
51. Skelton, N.J., Kördel, J., Akke, M. & Chazin, W.J. (1992). Nuclear magnetic resonance studies of the internal dynamics in apo, $(Cd^{2+})_1$ and $(Ca^{2+})_2$ calbindin D_{9k}. *J. Mol. Biol.* **227**, 1100–1117.
52. Laskowski, R.A., MacArthur, M.W., Moss, D.S. & Thornton, J.M. (1993). PROCHECK: a program to check stereochemical quality of protein structures. *J. Appl. Cryst.* **26**, 283–290.
53. Harris, N.L., Presnell, S.R. & Cohen, F.E. (1994). Four helix bundle diversity in globular proteins. *J. Mol. Biol.* **236**, 1356–1368.
54. Drohat, A.C., Nenortas, E., Beckett, D. & Weber, D.J. (1997). Oligomerization state of S100B at nanomolar concentration determined by large-zone analytical gel filtration chromatography. *Protein Sci.* **6**, 1577–1582.
55. Vijay-Kumar, S. & Cook, W.J. (1992). Structure of a sarcoplasmic calcium-binding protein from *Nereis diversicolor* refined at 2.0 Å resolution. *J. Mol. Biol.* **224**, 413–426.
56. Skelton, N.J., Kördel, J., Akke, M., Forsén, S. & Chazin, W. (1994). Signal transduction versus buffering activity in calcium-binding proteins. *Nat. Struct. Biol.* **1**, 239–245.
57. Marsden, B.J., Shaw, G.S. & Sykes, B.D. (1989). Calcium binding proteins. Elucidating the contributions to calcium affinity from analysis of species variants and peptide fragments. *Biochem. Cell Biol.* **68**, 587–601.
58. Satyshur, K.A., Rao, S.T., Pyzalska, D., Drendel, W., Greaser, M. & Sundaralingam, M. (1988). Refined structure of chicken skeletal muscle troponin C in the two-calcium state at 2 Å resolution. *J. Biol. Chem.* **263**, 1628–1647.
59. Strynadka, N.C.J. & James, M.N.G. (1989). Crystal structures of the helix-loop-helix calcium-binding proteins. *Annu. Rev. Biochem.* **58**, 951–998.

60. Baudier, J., Labourette, G. & Gerard, D. (1985). Rat brain S100b protein: purification, characterization and ion binding properties. A comparison with bovine S100b protein. *J. Neurochem.* **44**, 76–84.
61. Baudier, J. & Cole, R.D. (1989). The Ca-binding sequence in bovine brain S100b protein β-subunit. *Biochem. J.* **264**, 79–85.
62. Ivanenkov, V.V., Jamieson, G.A., Gruenstein, E. & Dimlich, R.V.W. (1995). Characterization of S-100b binding epitopes: identification of a novel target, the actin capping protein CapZ. *J. Biol. Chem.* **270**, 14651–14658.
63. Kube, E., Becker, T., Weber, K. & Gerke, V. (1992). Protein–protein interaction studied by site-directed mutagenesis: characterization of the annexin II binding site on p11, a member of the S100 protein family. *J. Biol. Chem.* **267**, 14175–14182.
64. Fohr, U.G., Heizmann, C.W., Engelkamp, D., Shäfer, B.W. & Cox, J.A. (1995). Purification and cation binding properties of the recombinant human S100 calcium-binding protein A3, an EF-hand motif protein with high affinity for zinc. *J. Biol. Chem.* **270**, 21056–21061.
65. Dell'Angelica, E.C., Schleicher, C.H. & Santome, J.A. (1994). Primary structure and binding properties of calgranulin C, a novel S100-like calcium-binding protein from pig granulocytes. *J. Biol. Chem.* **269**, 28929–28936.
66. Donato, H., Jr., Mani, R.S. & Kay, C.M. (1991). Spectral studies on the cadmium-ion-binding properties of bovine brain S-100b protein. *Biochem. J.* **276**, 13–18.
67. Kligman, D. & Marshak, D.R. (1985). Purification and characterization of a neurite extension factor from bovine brain. *Proc. Natl. Acad. Sci. USA* **82**, 7136–7139.
68. Winningham-Major, F., Staecker, J.L., Barger, S.W., Coats, S. & Van Eldik, L.J. (1989). Neurite extension and neuronal survival activities of recombinant S100β proteins that differ in the content and positions of cysteine residues. *J. Cell Biol.* **109**, 3063–3071.
69. Barger, S.W., Wolchok, S.R. & Van Eldik, L.J. (1992). Disulfide-linked S100β dimers and signal transduction. *Biochim. Biophys. Acta.* **1160**, 105–112.
70. Teigelkamp, S., Bhardwaj, R.S., Roth, J., Meinardus-Hager, G., Karas, M. & Sorg, C. (1991). Calcium-dependent complex assembly of the myeloic differentiation proteins MRP-8 and MRP-14. *J. Biol. Chem.* **266**, 13462–13467.
71. Wittekind, M. & Mueller, L. (1993). HNCACB, a high-sensitivity 3D NMR experiment to correlate amide–proton and nitrogen resonances with the alpha- and beta-carbon resonances. *J. Magn. Reson. Series B* **101**, 171–180.
72. Grzesiek, S. & Bax, A. (1992). Correlating backbone amide and sidechain resonances in larger proteins by multiple relayed triple resonance NMR. *J. Am. Chem. Soc.* **114**, 6291–6293.
73. Kay, L.E., Xu, G.Y. & Yamazaki, T. (1994). Enhanced-sensitivity triple-resonance spectroscopy with minimal H_2O saturation. *J. Magn. Reson. Series A* **109**, 129–133.
74. Zhang, O., Kay, L.E., Olivier, J.P. & Forman-Kay, J.D. (1994). Backbone ^1H and ^{15}N resonance assignments of the N-terminal SH3 domains of drk in the folded and unfolded states using enhanced-sensitivity pulsed field gradient NMR techniques. *J. Biolmol. NMR* **4**, 845–858.
75. Kay, L.E., Xu, G., Singer, A.U., Muhandiram, D.R. & Forman-Kay, J.D. (1993). A gradient-enhanced HCCH-TOCSY experiment for recording sidechain ^1H and ^{13}C correlations in H_2O samples of proteins. *J. Magn. Reson. Series B* **101**, 333–337.
76. Pascal, S.M., Muhandiram, D.R., Yamazaki, T., Forman-Kay, J.D. & Kay, L.E. (1994). Simultaneous acquisition of ^{15}N and ^{13}C-edited NOE spectra of proteins dissolved in H_2O. *J. Magn. Reson Series B* **103**, 197–201.
77. Macura, S. & Ernst, R.R. (1980). Elucidation of cross relaxation in liquids by two-dimensional NMR spectroscopy. *Mol. Phys.* **41**, 95–117.
78. Jeener, J., Meier, B.H., Bachmann, P. & Ernst, R.R. (1979). Investigation of exchange processes by two dimensional NMR spectroscopy. *J. Chem. Phys.* **71**, 4546–4553.
79. Delaglio, F. (1993). *NMRPipe System of Software.* National Institutes of Health, Bethesda, MD.
80. Garrett, D.S., Powers, R., Gronenborn, A.M. & Clore, G.M. (1991). A common sense approach to peak picking in two-, three-, and four-dimensional spectra using automatic computer analysis of contour diagrams. *J. Magn. Reson.* **95**, 214–220.
81. Kay, L.E., Keifer, P. & Saarinen, T. (1992). Pure absorption gradient enhanced heteronuclear single quantum correlation spectroscopy with improved Sensitivity. *J. Am. Chem. Soc.* **114**, 10663–10665.
82. Kuboniwa, H., Grzesiek, S., Delaglio, F. & Bax, A. (1994). Measurement of H^N-H^α J couplings in calcium-free calmodulin using new 2D and 3D water-flip-back methods. *J. Biomol. NMR* **4**, 871–878.
83. Vuister, G. & Bax, A. (1993). Quantitative J correlation: a new approach for measuring homonuclear three-bond $J(H^N$-$H\alpha)$ coupling constants in ^{15}N-enriched proteins. J. *Am. Chem. Soc.* **115**, 7772–7777.
84. Gagné, S.M., Li, M.X. & Sykes, B.D. (1997). Mechanism of direct coupling between binding and induced structural change in regulatory calcium binding proteins. *Biochemistry* **36**, 4386–4392.
85. Brünger, A.T. (1992). *X-PLOR version 3.1: A System for X-ray Crystallography and NMR.* Columbia University Press. New Haven, CT.
86. Nicholls, A. (1992). *GRASP: Graphical Representation and Analysis of Surface Properties.* Yale University Press, New York, NY.